



Article

Fabrication and Characterization of Granulated β -Tricalcium Phosphate and Bioactive Glass Powders by Spray Drying

Akihiro Nakanishi ^{1,2}, Henni Setia Ningsih ¹ , Dwi Fortuna Anjusa Putra ¹ , Toshihiro Moriga ²
and Shao-Ju Shih ^{1,*}

¹ Department of Materials Science and Engineering, National Taiwan University of Science and Technology, No. 43, Section 4, Keelung Road, Taipei 10607, Taiwan; c502043004@tokushima-u.ac.jp (A.N.); dwi.anjusa@gmail.com (D.F.A.P.)

² Department of Chemical Science and Technology, Graduate School of Advanced Technology and Science, Tokushima University, 2-1 Minami-Josanjima, Tokushima 770-8506, Japan; moriga@tokushima-u.ac.jp

* Correspondence: shao-ju.shih@mail.ntust.edu.tw; Tel.: +886-2-27303716

Abstract: Biocomposite materials are widely implemented in various applications in clinical dentistry and orthopedics since it is possible to combine multiple materials by relying on their compatibility. Ceramic-based materials have osteogenic and osteoconductive features owing to their inorganic constituents with dental and bone tissue. β -tricalcium phosphate (β -TCP) and bioactive glass have excellent biocompatibility, bioresorbability, and bioactivity. In this study, β -TCP and BG powders were fabricated by spray pyrolysis (SP) and spray drying (SD). These fabrication methods are suitable for the mass production and synthesis of spherical particles. At first, β -TCP and BG spherical particles were synthesized by SP and characterized using X-ray diffraction (XRD), Fourier transform infrared spectroscopy (FT-IR), and scanning electronic microscopy (SEM). After that, these powders were granulated with the different weight ratios of β -TCP/BG = 100/0, 75/25, 50/50, 25/75, and 0/100 by SD. The resulting granulation powders were characterized using XRD, FT-IR, and SEM to investigate phase compositions and microstructures. In addition, cytotoxicity was investigated using the MTT assay.

Keywords: β -tricalcium phosphate; bioactive glass; spray pyrolysis; spray drying; granulation



Citation: Nakanishi, A.; Ningsih, H.S.; Putra, D.F.A.; Moriga, T.; Shih, S.-J. Fabrication and Characterization of Granulated β -Tricalcium Phosphate and Bioactive Glass Powders by Spray Drying. *J. Compos. Sci.* **2024**, *8*, 111. <https://doi.org/10.3390/jcs8030111>

Academic Editors: Francesco Tornabene and Thanasis Triantafyllou

Received: 15 January 2024

Revised: 6 March 2024

Accepted: 14 March 2024

Published: 20 March 2024



Copyright: © 2024 by the authors. Licensee MDPI, Basel, Switzerland. This article is an open access article distributed under the terms and conditions of the Creative Commons Attribution (CC BY) license (<https://creativecommons.org/licenses/by/4.0/>).

1. Introduction

Bioceramics have recently garnered increasing attention due to their applications in the repair and reconstruction of bones [1]. Bioceramics with porous structures help improve mechanical strength at the interface between the bone and implant [2]. In addition, it provides a larger surface area and strong surface interaction between tissues and implants, along with good osteoinductive properties [3].

Calcium phosphate-based bioceramics have been widely used as implants for bone repair because they have similar chemical elements as human bones [4]. Calcium phosphate-based bioceramics include hydroxylapatite, α -tricalcium phosphate, β -tricalcium phosphate (β -TCP), and so on. Among these bioceramics, β -TCP bioceramics are popular due to their excellent biocompatibility [5,6] and superior bioresorbability [7].

Although β -TCP has become one of the potential candidates for bone implants, there is a critical problem of degradation behavior that needs to be overcome. β -TCP is a crystalline bioceramic material that has a constant degradation rate. Since young people have the fastest bone growth rate while older people have the slowest bone growth [8], β -TCP materials with fixed degradation behavior are not able to solve this problem. Therefore, new bone implants with a suitable personalized degradation rate are urgently required [9–11]. In order to propose a possible solution for personalized bone grafts, β -TCP and bioactive glass (BG)-composited materials were studied. BG-based materials, with an amorphous structure, are adjustable in chemical composition and, therefore, offer adjustable degradation rates [12,13]. Also, BG is currently attracting attention due to its ability to react

chemically on the material surface and bond directly to the surrounding tissue. BG, first discovered by Hench in 1969 [14,15], forms inorganic-like thin layers of hydroxyapatite (HAp) at the junction with bone through which it spontaneously bonds. The degradation rate of pure β -TCP material is faster than that of β -TCP/BG-composited materials [16].

According to previous studies, β -TCP and BG composites are commonly synthesized by the sol–gel method, i.e., Spirandeli et al. [17] reported that the β -TCP and BG composites through the sol–gel method need high calcination temperatures and have uneven particle size. Therefore, it is worth considering other fabrication methods. Spray pyrolysis (SP) is a good choice because of its large amount, uniformity, and lower synthetic temperature compared to the sol–gel method [18–21]. Spray drying (SD) is a technique that transforms liquid into powders, offering an effective way to fabricate not only porous structures but also composites. It has some advantages, such as cost-effectiveness, mass production, and controllable morphology [22–25]. In addition, the resulting particles have a narrow size distribution and are spherical, microsphere, or granular in shape and are non-agglomerated [26]. There are two distinct groups of ceramic microspheres as follows: (i) those with dense and smooth granules with high density, specific surface area, and strong compatibility; (ii) those with hollow or porous granules with a high specific surface area [27]. SP-derived spherical particles (particle size of $\sim 1 \mu\text{m}$) may help SD-derived-granulated powder become more uniform and denser because the spherical particles are likely to form closed-packing.

In this study, the starting powders of β -TCP and BG particles were synthesized by SP. The phase compositions and particle morphologies of these starting powders were characterized using X-ray diffraction (XRD) and scanning electron microscopy (SEM), respectively. After that, these starting powders were granulated with various weight% ratios of β -TCP/BG = 100/0, 75/25, 50/50, 25/75, and 0/100 using SD. The phase compositions of these five granulated powders were measured by XRD; Fourier transform infrared spectroscopy and SEM was employed to investigate the corresponding bonding structures and microstructures, respectively. In addition, the cytotoxicity of each granulated powder was investigated via the MTT assay.

2. Materials and Methods

2.1. Preparation and Characterization of β -TCP and BG Starting Powders

In this work, β -TCP and BG powders were fabricated by spray pyrolysis (SP). Initially, the β -TCP powders were prepared following our previous study [19] with the molar ratio of Ca/P at 3:2. Calcium nitrate tetrahydrate (CNT, $\text{Ca}(\text{NO}_3)_2 \cdot 4\text{H}_2\text{O}$, 98.5%, Showa, Tokyo, Japan) and diammonium hydrogen phosphate (DHP, $(\text{NH}_4)_2\text{HPO}_4$, 98.0%, Thermo Fisher Scientific, Waltham, MA, USA) were used as the sources of Ca and P. The precursor solution was prepared by mixing 70.84 g of CNT and 26.42 g of DHP in 500 mL of deionized (DI) water. After stirring for 30 min, 10 mL of nitric acid (HNO_3 , 69.5%, Scharlau, Barcelona, Spain) was added dropwise to adjust the pH to 3. Afterward, the precursor solutions were stirred for 12 h at room temperature to obtain a uniform and transparent β -TCP precursor solution. Next, for BG powders ($\text{SiO}_2:\text{CaO}:\text{P}_2\text{O}_5 = 80:15:5$ in mol%), the initial precursor solution was prepared by mixing 21.79 g of CNT, 96.15 g of tetraethyl orthosilicate (TEOS, $\text{Si}(\text{OC}_2\text{H}_5)_4$, 98%, Thermo Fisher Scientific, Waltham, MA, USA) and 8.23 g of triethyl phosphate (TEP, $(\text{C}_2\text{H}_5)_3\text{PO}_4$, 99 wt %, Alfa Aesar, Haverhill, MA, USA) with 120 g of ethanol. After stirring for 30 min, DI water was added to bring the volume to 1 L, and 10 mL of 0.5 M hydrochloric acid (HCl) was added to adjust the pH to 2.5. Then, the mixture solutions were stirred for another 12 h in order to obtain uniform and transparent BG precursor solutions. For the spray pyrolysis (SP) process, the prepared precursor solutions were atomized into droplets by an ultrasonic atomizer (King Ultrasonic, KT-100A, New Taipei, Taiwan) with a frequency of 1.65 MHz. Next, the resulting droplets were fed into a quartz tube furnace (with a length of 1200 mm and diameter of 30 mm) with the heating temperatures shown in Table 1. Finally, the resulting powders were collected in an earthed stainless tube and dried in an oven for 1 day.

Table 1. The temperature settings of three heating zones for β -TCP and BG starting powders by SP.

	Pre-Heating (°C)	Calcination (°C)	Cooling (°C)
β -TCP	300	1050	350
BG	400	700	500

2.2. Characterization of β -TCP and BG Starting Powders

For characterization, the phase composition of β -TCP and BG powders was confirmed by X-ray diffraction (XRD, D2 Phaser, Bruker, Karlsruhe, Germany) with Cu-K α radiation at 30 kV and 2θ in the range of 20–80°. The functional groups of β -TCP and BG powders were investigated using Fourier transform infrared spectroscopy (FT-IR, Digilab FTS-3500, Agilent, Santa Clara, CA, USA) at room temperature with the transmittance mode in the wave number range from 400 cm⁻¹ to 1300 cm⁻¹. Before the measurement, the samples and KBr with a weight ratio of 1.4 mg and 100 mg were mixed using mortar; then, 20 mg of the mixed powders were weighed and pressed to make a pellet by the die-pressing technique. Finally, the morphologies and particle sizes were observed for more than 300 particles in several micrographs using field emission scanning electron microscopy (JSM-6500, JEOL, Tokyo, Japan).

2.3. Preparation of Granulated β -TCP/BG Powders

For the fabrication of granulated β -TCP/BG powders, the slurries were prepared by adding 1.3 g of poly-N-vinyl acetamide (PNVA, 13.0%, Showa, Tokyo, Japan) as a dispersant and 26.0 g of spray-pyrolyzed β -TCP/BG powders with various weight ratios of β -TCP/BG at 100/0, 75/25, 50/50, 25/75, and 0/100 into 50.0 mL of DI water. Meanwhile, for the binder solutions, 1.3 g of polyvinyl alcohol (PVA, 88%, M. W. 20,000–30,000, Thermo Fisher Scientific, Waltham, MA, USA) and 30.0 mL of DI water were stirred at 50 °C for 1 h. Next, slurry and binder solutions were mixed with the addition of 21.4 mL of DI water and stirred for 12 h. The detailed amount of all reagents is listed in Table 2.

Table 2. The amount of reagent for granulation slurry.

Sample (Weight Ratio: β -TCP/BG)	β -TCP (g)	BG (g)	PVA (g)	PNVA (g)	Water (g)	Total (g)
100/0	26	0	1.3	1.3	101.4	130
75/25	19.5	6.5	1.3	1.3	101.4	130
50/50	13	13	1.3	1.3	101.4	130
25/75	6.5	19.5	1.3	1.3	101.4	130
0/100	0	26	1.3	1.3	101.4	130

Finally, for the spray drying process, the final slurry was introduced into the spray dryer (SDDO-03, IDTA machinery Co., New Taipei, Taiwan) with a flow rate of ~20 mL/min and a high-speed-rotating disc at 20,000 rpm. The inlet and outlet temperatures were set at 200 °C and 75 °C, respectively. The obtained powders were calcined at 400 °C for 2 h to remove the dispersants and binders.

2.4. Characterization of Granulated β -TCP/BG Powders

The crystalline structures of granulated β -TCP/BG powders were investigated using XRD. The crystalline size was calculated using Scherrer's equation as follows:

$$D = \frac{K\lambda}{B\cos\theta} \quad (1)$$

where D is the crystallite size, K is the Scherrer constant, the value of which is 0.89 [28], λ is the wavelength of the Cu-K α radiation, B is the full width at half maximum (FWHM) of the peak, and θ is the diffraction angle. The morphologies and average particle sizes were studied by SEM (JSM-6500, JEOL, Tokyo, Japan) with an operating voltage of 15 kV.

Before the measurement, the samples were placed on the carbon tape in an SEM holder and coated with the conductive metal. The average particle size distributions were obtained by counting more than 300 particles for each sample using ImageJ 1.50i software. Moreover, the coefficient of variation (COV) was used to identify the variation in all granulated β -TCP/BG powder distribution sizes, which was calculated using the equation below:

$$COV = \frac{SD}{D_{avg}} \times 100\% \quad (2)$$

where SD denotes the standard deviation and D_{avg} denotes the average sphere size. The functional groups of granulated β -TCP/BG were investigated using Fourier transform infrared spectroscopy (FT-IR, Digilab FTS-3500, Agilent, Santa Clara, CA, USA) at room temperature with the transmittance mode in the wave number range from 400 cm^{-1} to 1300 cm^{-1} .

Finally, the cell viability of granulated β -TCP/BG powders was investigated via the MTT assay. The MC3T3-E1 cells (ATCC CRL-2594, Manassas, VA, USA) were cultured in MEM- α (Gibco, Waltham, MA, USA) containing 1% penicillin–streptomycin (Thermo Fisher, Waltham, MA, USA) and 10% FBS (Gibco, Waltham, MA, USA) in a humidified 5% CO_2 atmosphere incubator at $36.5\text{ }^\circ\text{C}$ for 24 h. The MEM- α -containing granulated β -TCP/BG powder with a dilution concentration of 100 mg/mL was added and incubated for 72 h. Afterward, the MEM- α was removed, and $300\text{ }\mu\text{L}$ of the MTT solution (Alfa Aesar, Haverhill, MA, USA) solution was added to each well. After 4 h, the MTT solution was removed, and $200\text{ }\mu\text{L}$ of dimethyl sulfoxide (DMSO, Echo, Taipei, Taiwan) was added to dissolve the formazan crystal. Finally, the absorbance of the solution was measured at 570 nm with a microplate reader (Multiskan Go, Thermo Scientific, Waltham, MA, USA). The cell viability of each concentration was calculated with reference to the control solution without a sample.

2.5. Statistical Analysis

The results of cell viability were expressed as the mean \pm standard deviation, with sample $n = 3$. Statistical analysis was determined using the t -test, where a statistically significant difference was considered at p -value < 0.05 and denoted as *.

3. Results

3.1. SP-Derived β -TCP and BG Starting Powders

In this work, various granulated β -TCP/BG powders were fabricated with a two-step process. First, the starting β -TCP and BG powders were synthesized by SP (described in this section), and then the as-received β -TCP and BG powders were granulated using SD. The XRD patterns of as-received β -TCP and BG powders are shown in Figure 1. Initially, for the β -TCP powder, the crystalline phase with 28 diffraction peaks was detected within the diffraction angle 2θ range of $20\sim 80^\circ$, indicating a single phase of β -TCP (JCPDS No. 09-0169). Next, the XRD pattern of BG powder showed a broad peak at $2\theta\sim 20\text{--}40^\circ$, which demonstrated the amorphous phase of BG. In brief, the XRD results suggest the presence of crystalline in the β -TCP powder, whereas the BG powder exhibits an amorphous phase.

Figure 2 depicts the FT-IR spectra of as-received β -TCP and BG powders. The first peak at $450\text{--}500\text{ cm}^{-1}$ is for the O-Si-O/Si-O-Si angle bending vibration. Additionally, the peak at 800 cm^{-1} is due to the vibration of the Si^{4+} cation within the SiO_4 tetrahedron [18,29]. The O-P-O ν_4 bending vibration of phosphate groups is evident due to the peak at $550\text{--}650\text{ cm}^{-1}$ [18,30]. The transmittance peak around $940\text{--}1150\text{ cm}^{-1}$ was detected in both as-received β -TCP and BG powders because the silicate and phosphate peaks coexisted. The peak around 1100 cm^{-1} comes from asymmetric Si-O stretching. The other peaks around $940\text{--}1050\text{ cm}^{-1}$ and 1130 cm^{-1} come from the stretching mode of the PO_4 group [18,29,31]. In short, the FT-IR result demonstrates that as-received β -TCP and BG powders have the main features of β -TCP and BG.

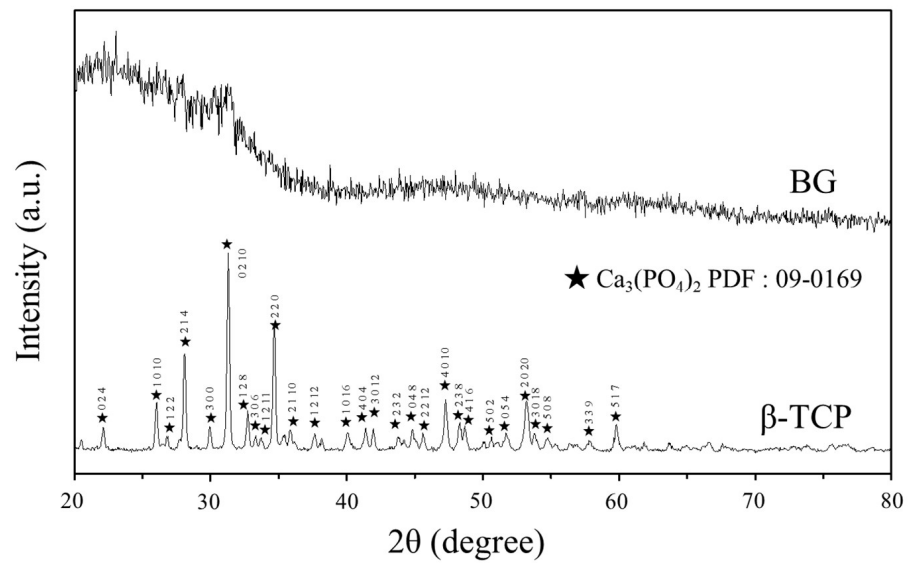


Figure 1. XRD patterns of SP-derived β -TCP and BG powders.

The SEM images of SP-derived β -TCP and BG powders are shown in Figure 3. The average particle size and the standard deviations of β -TCP and BG powders were $1.37 \pm 0.57 \mu\text{m}$ and $1.06 \pm 0.54 \mu\text{m}$, respectively. From the SEM image, it was observed that there are three types of morphologies, including smoothed (type 1), roughed (type 2), and concaved particles (type 3). Figure 4 shows the populations of the three typical morphologies for the β -TCP and BG powders. In the case of SP-derived β -TCP powders, all types of particle shapes were identified. The frequencies of type 1, type 2, and type 3 particles were 35%, 26%, and 39%, respectively. In the case of BG, the populations of type 1, type 2, and type 3 particles were 93%, 7%, and 0%, respectively. In brief, for SP-derived β -TCP, the populations of type 1, type 2, and type 3 particles were similar; however, the proportion of type 1 particles comprised the majority for SP-derived BG powders.

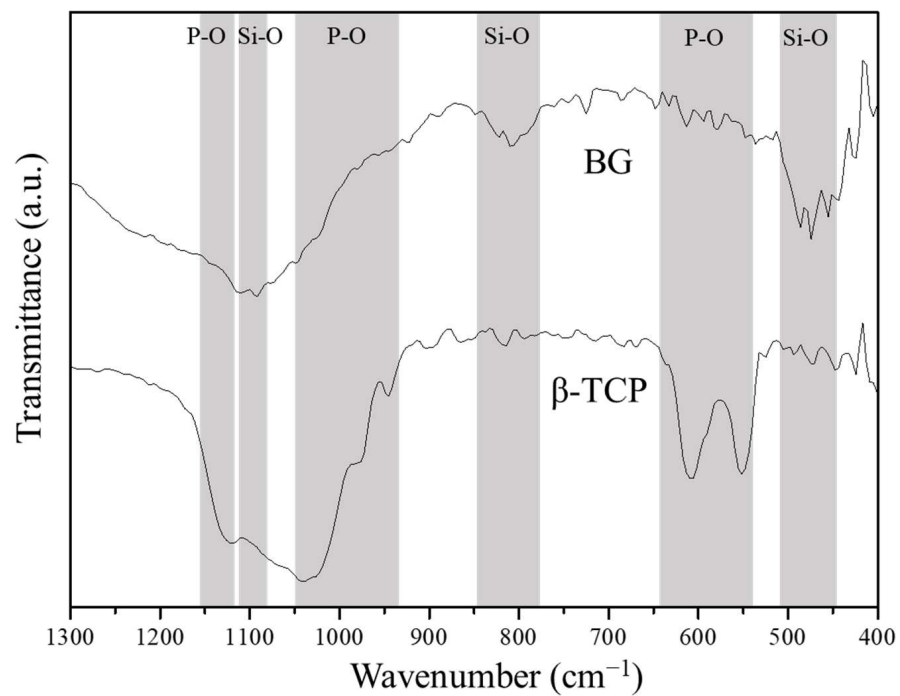


Figure 2. FTIR spectra of SP-derived β -TCP and BG powders.

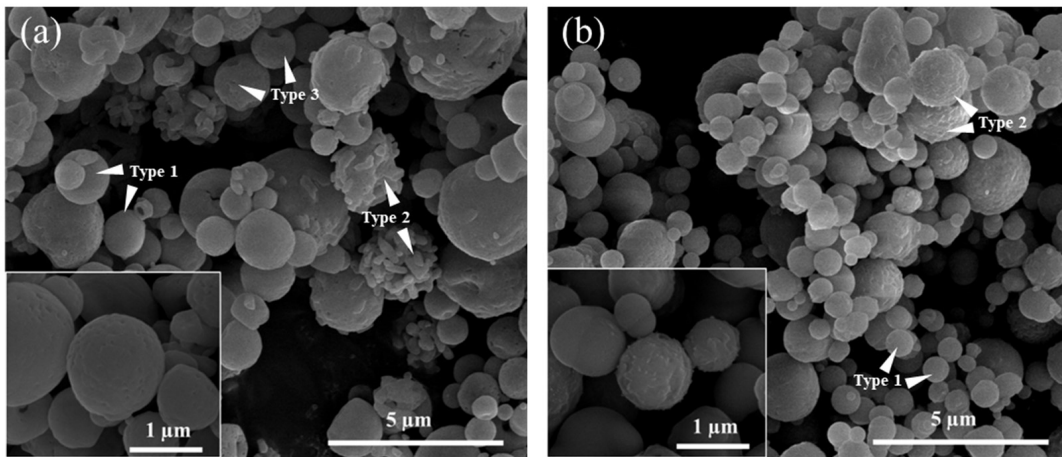


Figure 3. SEM images of SP-derived (a) β -TCP and (b) BG powders.

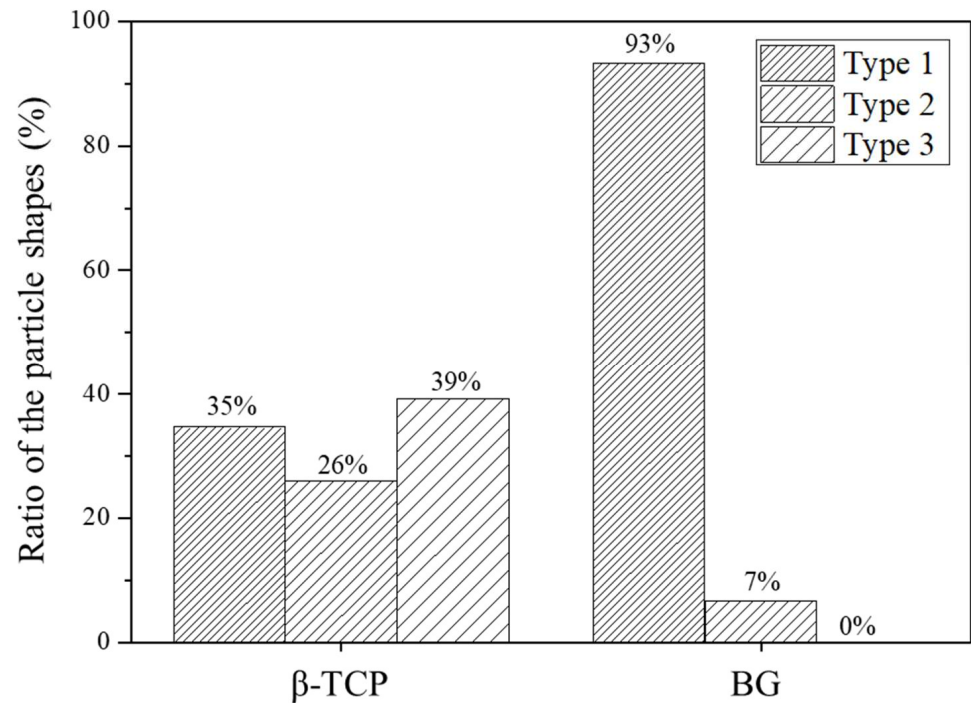


Figure 4. The ratio of the particle shapes of β -TCP and BG powders from the statistical analysis.

3.2. Granulated β -TCP/BG Powders

The XRD patterns of granulated β -TCP/BG powders (weight ratio: β -TCP/BG = 100/0, 75/25, 50/50, 25/75, and 0/100) are shown in Figure 5. The four granulated β -TCP/BG powders with the weight ratios of β -TCP/BG = 100/0, 75/25, 50/50, and 25/75) all exhibit the crystalline phase of β -TCP (JCPDF No. 09-0169), which reveals the existence of SP derived- β -TCP-starting particles. Also, the granulated β -TCP/BG powder (weight ratio: β -TCP/BG = 0/100) reveals an amorphous phase. With of the increase in the BG ratio, the intensities of β -TCP diffraction peaks decrease, and the broad peak from BG at the 2θ angle of $\sim 20\text{--}40^\circ$ becomes stronger. The crystallite sizes of granulated β -TCP/BG powders are 47.7 ± 1.0 nm (β -TCP/BG = 100/0), 33.1 ± 1.8 nm (β -TCP/BG = 75/25), 34.4 ± 1.9 nm (β -TCP/BG = 50/50), and 36.8 ± 0.2 nm (β -TCP/BG = 25/75). In summary, the crystalline sizes of BG-including granulated powders are smaller than that of pure β -TCP-granulated powder.

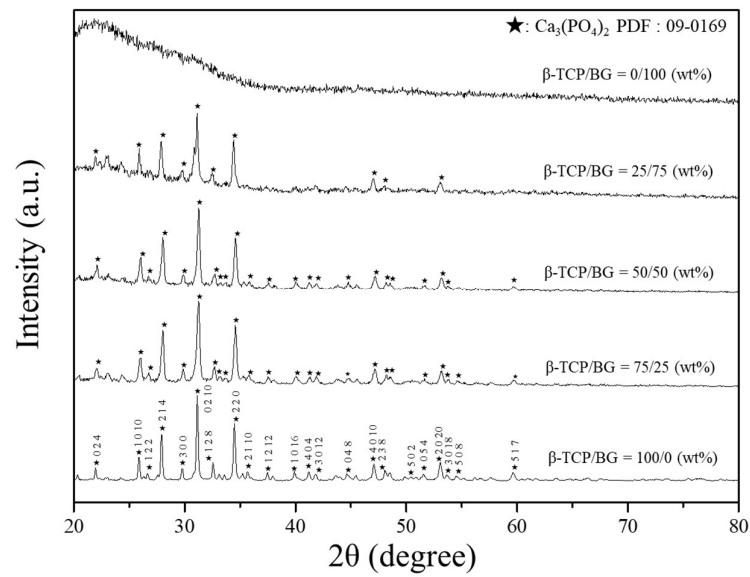


Figure 5. XRD patterns of SD-granulated powders with the different weight% ratios of β -TCP/BG = 100/0, 75/25, 50/50, 25/75, and 0/100.

In addition, the FT-IR spectra of granulated β -TCP/BG powders are shown in Figure 6. The transmittance peaks around $450\text{--}500\text{ cm}^{-1}$ and 800 cm^{-1} gradually appeared with the increasing ratio of BG. The peak around $450\text{--}500\text{ cm}^{-1}$ came from the O-Si-O/Si-O-Si angle bending vibration. The peak at around 800 cm^{-1} came from the vibration of the Si^{4+} cation within the SiO_4 tetrahedron [18,29]. In addition, the peak around $550\text{--}650\text{ cm}^{-1}$ gradually disappeared with the increasing ratio of BG. This peak came from the O-P-O ν_4 bending vibration of phosphate groups [18,30]. The transmittance peak around $940\text{--}1150\text{ cm}^{-1}$ was detected regardless of the ratio of β -TCP and BG because the silicate and phosphate peaks coexisted. The peak around 1100 cm^{-1} came from asymmetric Si-O stretching. The peaks around $940\text{--}1050\text{ cm}^{-1}$ and 1130 cm^{-1} came from the stretching mode of the PO_4 group [18,29,31]. In summary, the FT-IR spectra of all granulated β -TCP/BG powders are consistent with the FT-IR spectra of as-received β -TCP and BG powders.

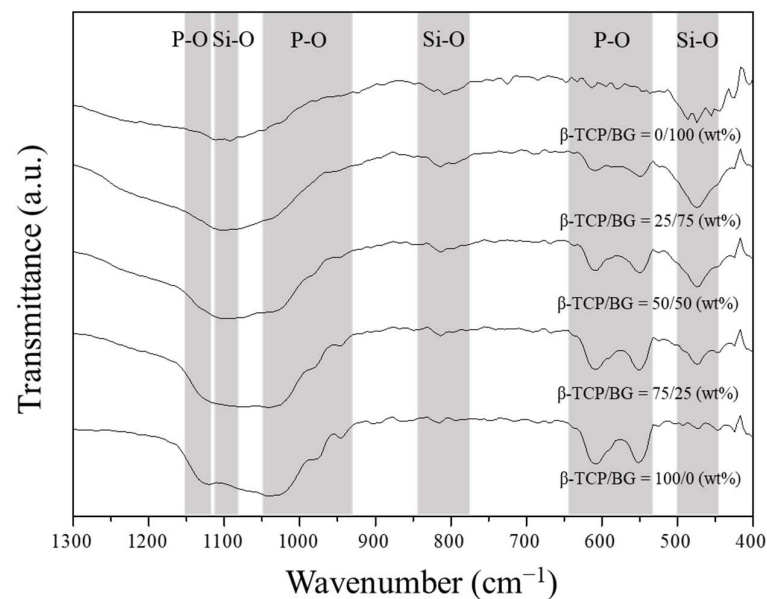


Figure 6. FTIR spectra of SD-granulated powders with the different weight% ratios of β TCP/BG = 100/0, 75/25, 50/50, 25/75, and 0/100.

The SEM images of granulated β -TCP/BG powders are shown in Figure 7. As observed, the granulated β -TCP/BG powders are nearly spherical particles. The particle size distributions of granulated β -TCP/BG powders are shown in Figure 8. As can be seen, the average particle size and its error range were $25.56 \pm 7.11 \mu\text{m}$ (β -TCP/BG = 100/0), $26.62 \pm 7.16 \mu\text{m}$ (β -TCP/BG = 75/25), $25.74 \pm 6.93 \mu\text{m}$ (β -TCP/BG = 50/50), $28.57 \pm 8.26 \mu\text{m}$ (β -TCP/BG = 25/75), and $23.39 \pm 4.88 \mu\text{m}$ (β -TCP/BG = 0/100). In summary, the particle sizes of all granulated β -TCP/BG powders are around $25 \mu\text{m}$. The obtained coefficients of variation values were 27.82%, 26.89%, 26.92%, 28.91%, and 20.86% for the 100/0, 75/25, 50/50, 25/75, and 0/100 granulated β -TCP/BG powders, respectively. These results show that all granulated β -TCP/BG powders had consistent distributions.

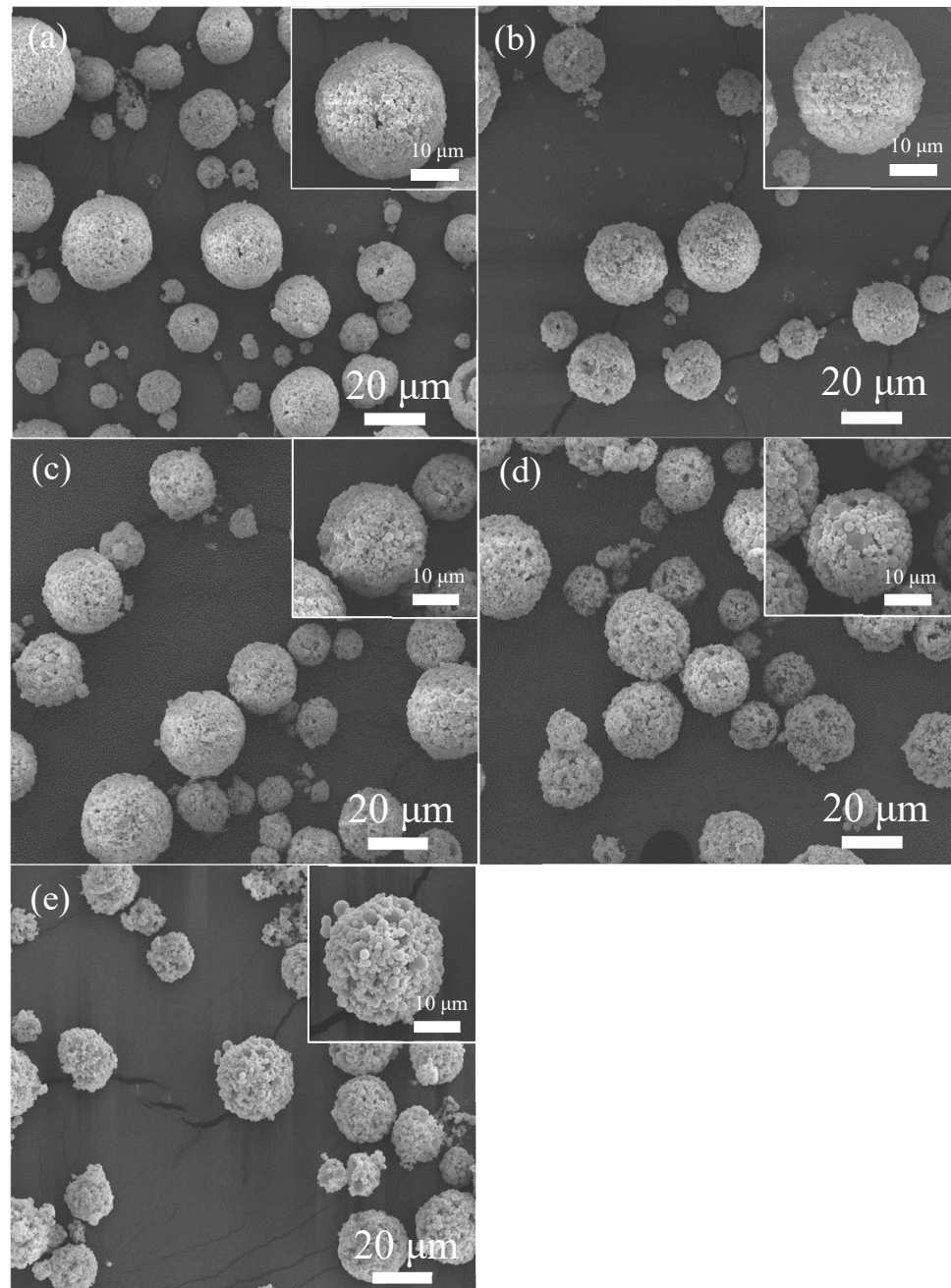


Figure 7. SEM images of SD-granulated powders with the different weight% ratios of β -TCP/BG (a) 100/0, (b) 75/25, (c) 50/50, (d) 25/75, and (e) 0/100.

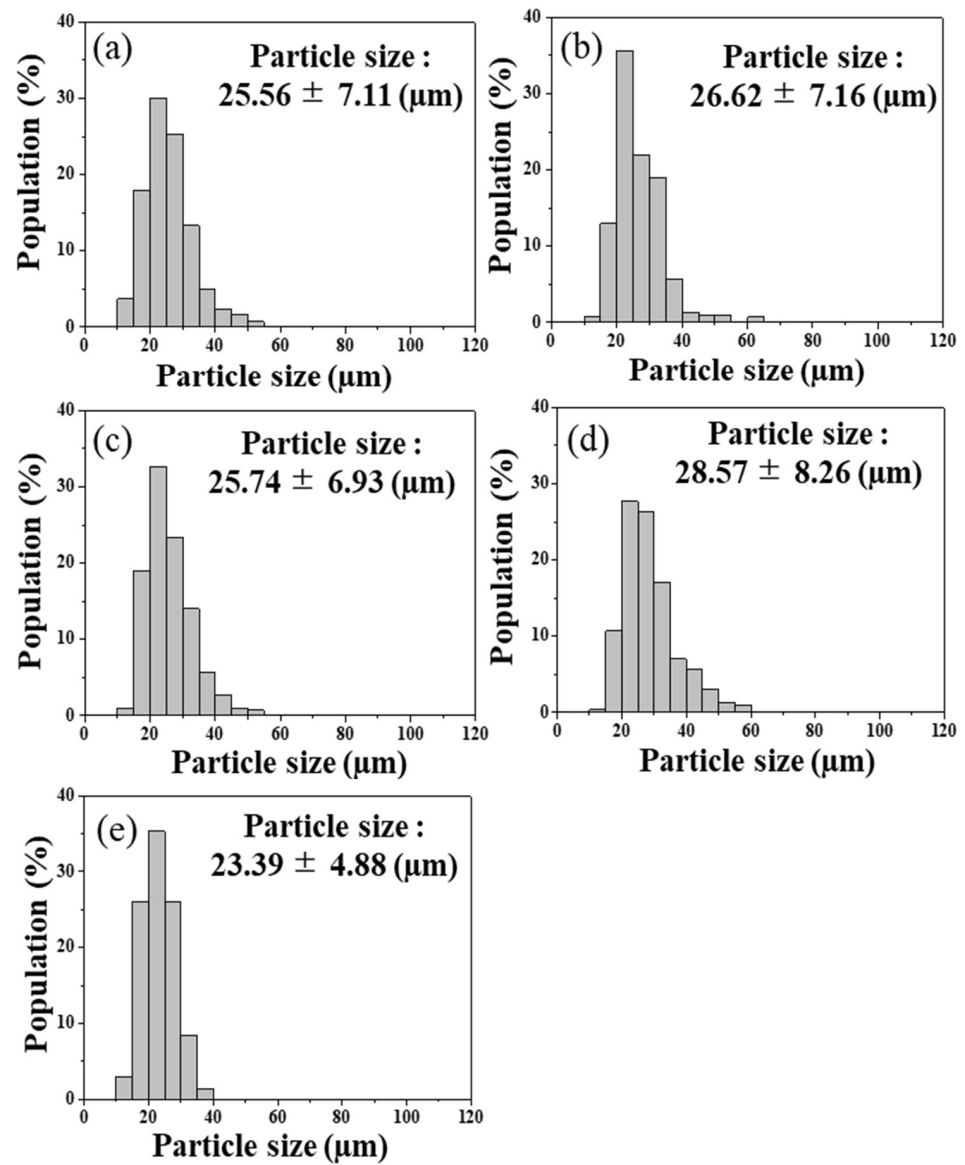


Figure 8. Particle size distributions of SD-granulated powders with the different weight% ratios of β -TCP/BG (a) 100/0, (b) 75/25, (c) 50/50, (d) 25/75, and (e) 0/100.

3.3. Cytotoxicity Test

The cell viability test of granulation powders derived from the MC3T3-E1 cell after 3 days of incubation is shown in Figure 9. The average cell viability and the corresponding error ranges of granulated β -TCP/BG powders are $129.8 \pm 8.2\%$, $106.1 \pm 1.3\%$, $107.4 \pm 1.7\%$, $91.2 \pm 1.1\%$, and $93.8 \pm 8.3\%$ for β -TCP/BG = 100/0, 75/25, 50/50, 25/50, 0/100, respectively. According to ISO 10993-5 [32], all granulated β -TCP/BG powders have cell viability above 70%, which indicates that all granulated samples are non-toxic.

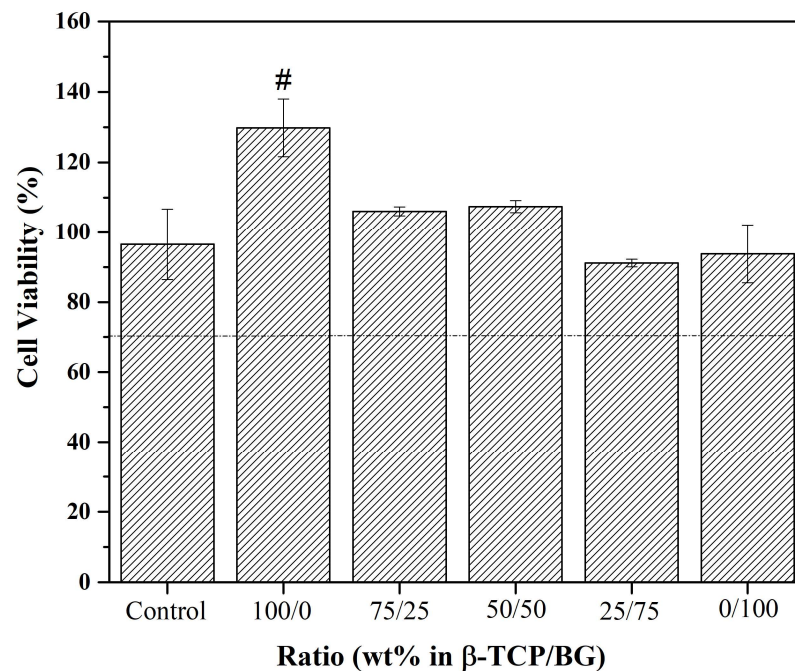


Figure 9. The cell viability of SD-granulated powders with the different weight% ratios of β -TCP/BG = 100/0, 75/25, 50/50, 25/75, and 0/100 after 3 days of incubation. The concentration of samples is 25 mg/mL (# presents the statistical differences with respect to the control, $n = 3$, and $p < 0.05$).

4. Discussion

First, let us discuss the morphologies of SP-derived β -TCP and BG starting powders. Based on SEM images, as shown in Figure 3, diverse morphologies were observed involving smoothed, roughed, and concaved spheres. The distributions of these morphological types are illustrated in Figure 3. The variations in morphology can be affected by many factors, such as the coefficient of thermal expansion (CTE), precursor solutions, and calcination temperature [18,23]. Firstly, to be noted, CTE is defined as the degree of change in length or volume in response to a temperature change [33,34]; this is considered because the rapid thermal expansion may cause cracking in the material. Materials with a larger CTE are more sensitive to heat and are likely to change their length or volume. The CTE values of β -TCP and BG are $1.47 \times 10^{-5} \text{ K}^{-1}$ and $1.50 \times 10^{-5} \text{ K}^{-1}$ [31,33], respectively. The CTE values of BG and β -TCP are similar, which suggests that the CTE may not dominate the particle morphology in this study. Secondly, for the precursor solution factor, the concaved sphere morphologies obtained from SP-derived β -TCP powder can be related to the presence of nitric acid as the catalyst in the precursor solution. Nitric acid leads to the release of NO_3 gas during the decomposition stage in the SP process, which may damage the spherical structure to form a concave structure [18,23]. The third factor is the calcination temperature. It is well known that the mechanism of precipitation of the droplets produced by SP affects the final particle shape. There are two precipitation mechanisms [21] as follows: volume precipitation and surface precipitation (see Figure 10). Volume precipitation occurs easily at a lower calcination temperature because of the slow evaporation of the solvent; the smaller temperature difference between the center and the surface of the droplet leads to solid particles because of the uniform precipitation within the droplets. For example, in this study, BG particles mainly had smooth surfaces (93% of the total particles) due to the volume precipitation at a lower calcination temperature (700 °C). On the other hand, in this study, surface precipitation occurred at a higher temperature because of the rapid evaporation of the solvent from the surface of droplets. In the case of β -TCP, more than half of the particles (65%) belonged to rough (Type 2) or concave (Type 3) particles due to the surface precipitation at a higher calcination temperature (1050 °C).

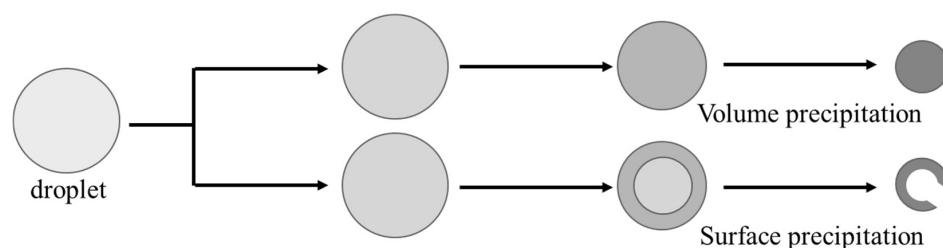


Figure 10. The mechanisms of volume precipitation and surface precipitation in SP.

Next, the formation mechanism of granulated β -TCP/BG powders is discussed below. According to the SEM images and granulated size distributions, as shown in Figures 7 and 8, the results show that all granulated β -TCP/BG powders exhibit spherical morphology with similar granulated size distributions at around 25 μm . This is owing to the typical spray granulation mechanism. The atomization process is necessary to expand the surface area of the slurry in SD because faster heat transfer occurs between the surface of the droplet and the drying medium. After the atomization process, the evaporation of the solvent from the produced droplet occurs due to the temperature and vapor pressure difference between the surface of the droplet and the drying medium [35]. During the SD granulation process, the slurry is atomized into droplets and then dried into spherical particles. For the preparation of the slurry, a dispersant is used to stabilize the slurry. The binder is also necessary to enhance cohesive strength for fluidity [27]. However, the excessive dosing of the binder may not result in spherical particles due to particle agglomeration [22]. In this study, spherical granulated particles were successfully obtained under slurry contents with a 20 wt % solid content, 1 wt % dispersant, and 1 wt % binder. Briefly, the SEM images confirmed that all granulated β -TCP/BG powders went through the typical spray granulation mechanism and resulted in consistent sphere size distributions.

Finally, the cell viability of granulated β -TCP/BG powders is discussed. All granulated β -TCP/BG powders have a cell viability above 70%, which indicates that all samples are non-toxic. According to previous studies, cytotoxicity is affected by the specific surface area [36]. Particles that are nano-sized have a larger specific surface area and might demonstrate toxicity due to more active sites on which particles can interact with cells [37]. In our study, all granulated β -TCP/BG powders did not exhibit toxicity, implying a non-nano structure. In addition, the cell viability of granulated β -TCP/BG powders (weight ratio: β -TCP/BG = 100/0, 75/25, and 50/50) was above 100%, indicating the promotion of cell viability. It is reported that pure β -TCP promotes cell viability, and the side product $\text{Ca}_2\text{P}_2\text{O}_7$ inhibits the mineralization of osteoblast cultures [36,38]. In this study, the granulated β -TCP/BG powders were obtained using SD without the formation of the side product $\text{Ca}_2\text{P}_2\text{O}_7$; this confirms the suitability of the powders for bone implant application.

5. Conclusions

In this study, β -TCP and BG powders with particle sizes of 1.37 μm and 1.06 μm , respectively, were prepared by SP. The morphology difference between β -TCP and BG particles came from the difference in the calcination temperature and precursor solution of the products. In addition, different weight ratios of β -TCP- and BG-granulated powders were successfully obtained by SD. The granulated β -TCP/BG powders with variance weight ratios of β -TCP/BG had spherical morphology with particle sizes at around 25 μm . Moreover, the cell viability showed the significant promotion of the granulated pure β -TCP sample on the proliferation of the MC3T3-E1 osteoblast cells. All granulated β -TCP/BG samples showed great potential for application in bone implants.

Author Contributions: Conceptualization, S.-J.S.; methodology, A.N. and D.F.A.P.; validation, S.-J.S. and H.S.N.; formal analysis, A.N. and H.S.N.; investigation, A.N.; data curation, A.N.; writing—original draft preparation, A.N.; writing—review and editing, S.-J.S. and H.S.N.; supervision, S.-J.S.; project administration, S.-J.S.; funding acquisition, S.-J.S. and T.M. All authors have read and agreed to the published version of the manuscript.

Funding: This research was funded by financial support from the Tokushima University and National Taiwan University of Science and Technology, Taiwan (Grant Numbers of TU-NTUST-110-06 and TU-TaiwanTech-2022-2).

Data Availability Statement: All datasets are publicly available.

Conflicts of Interest: The authors declare no conflicts of interest.

References

1. Brunello, G.; Panda, S.; Schiavon, L.; Sivolella, S.; Biasetto, L.; Del Fabbro, M. The impact of bioceramic scaffolds on bone regeneration in preclinical in vivo studies: A systematic review. *Materials* **2020**, *13*, 1500. [[CrossRef](#)] [[PubMed](#)]
2. Hench, L.L. Bioceramics: From concept to clinic. *J. Am. Ceram. Soc.* **1991**, *74*, 1487–1510. [[CrossRef](#)]
3. Ji, L.; Jell, G.; Dong, Y.; Jones, J.R.; Stevens, M.M. Template synthesis of ordered macroporous hydroxyapatite bioceramics. *Chem. Commun.* **2011**, *47*, 9048–9050. [[CrossRef](#)] [[PubMed](#)]
4. Eliaz, N.; Metoki, N. Calcium phosphate bioceramics: A review of their history, structure, properties, coating technologies and biomedical applications. *Materials* **2017**, *10*, 334. [[CrossRef](#)] [[PubMed](#)]
5. Gomes, D.; Santos, A.; Neves, G.; Menezes, R. A brief review on hydroxyapatite production and use in biomedicine. *Cerâmica* **2019**, *65*, 282–302. [[CrossRef](#)]
6. Zhao, R.; Yang, R.; Cooper, P.R.; Khurshid, Z.; Shavandi, A.; Ratnayake, J. Bone grafts and substitutes in dentistry: A review of current trends and developments. *Molecules* **2021**, *26*, 3007. [[CrossRef](#)] [[PubMed](#)]
7. Eggli, P.; Moller, W.; Schenk, R. Porous hydroxyapatite and tricalcium phosphate cylinders with two different pore size ranges implanted in the cancellous bone of rabbits: A comparative histomorphometric and histologic study of bony ingrowth and implant substitution. *Clin. Orthop. Relat. Res.* **1988**, *232*, 127–138. [[CrossRef](#)]
8. Cai, S.; Xu, G.; Yu, X.; Zhang, W.; Xiao, Z.; Yao, K. Fabrication and biological characteristics of β -tricalcium phosphate porous ceramic scaffolds reinforced with calcium phosphate glass. *J. Mater. Sci. Mater. Med.* **2009**, *20*, 351–358. [[CrossRef](#)]
9. Hsu, P.-Y.; Kuo, H.-C.; Syu, M.-L.; Tuan, W.-H.; Lai, P.-L. A head-to-head comparison of the degradation rate of resorbable bioceramics. *Mater. Sci. Eng. C* **2020**, *106*, 110175. [[CrossRef](#)]
10. Lin, H.-Y.; Huang, Y.-K.; Hsu, P.-Y.; Tuan, W.-H.; Naito, M. Sintering of degradable bone substitutes at room temperature. *Ceram. Int.* **2021**, *47*, 21714–21720. [[CrossRef](#)]
11. Uzun Kart, E. A Novel Method to Synthesis of Calcium Sulphate Anhydrite Self-Doped with SiO₂ from Red Mud as a Bioceramic. *Ceram. Silik.* **2021**, *65*, 344–353. [[CrossRef](#)]
12. Chou, Y.-J.; Hsiao, C.-W.; Tsou, N.-T.; Wu, M.-H.; Shih, S.-J. Preparation and in vitro bioactivity of micron-sized bioactive glass particles using spray drying method. *Appl. Sci.* **2018**, *9*, 19. [[CrossRef](#)]
13. Rahaman, M.N.; Day, D.E.; Bal, B.S.; Fu, Q.; Jung, S.B.; Bonewald, L.F.; Tomsia, A.P. Bioactive glass in tissue engineering. *Acta Biomater.* **2011**, *7*, 2355–2373. [[CrossRef](#)]
14. Hench, L.L.; Splinter, R.J.; Allen, W.; Greenlee, T. Bonding mechanisms at the interface of ceramic prosthetic materials. *J. Biomed. Mater. Res.* **1971**, *5*, 117–141. [[CrossRef](#)]
15. Jones, J.R. Review of bioactive glass: From Hench to hybrids. *Acta Biomater.* **2013**, *9*, 4457–4486. [[CrossRef](#)]
16. Xin, F.; Chen, J.; Ruan, J.; Zhou, Z.; Zou, J. Synthesis and degradation properties of TCP/BG porous composite materials. *Bull. Mater. Sci.* **2011**, *34*, 357–364. [[CrossRef](#)]
17. Spirandeli, B.; Ribas, R.; Amaral, S.; Martins, E.; Esposito, E.; Vasconcellos, L.; Campos, T.; Thim, G.; Trichês, E. Incorporation of 45S5 bioglass via sol-gel in β -TCP scaffolds: Bioactivity and antimicrobial activity evaluation. *Mater. Sci. Eng. C* **2021**, *131*, 112453. [[CrossRef](#)] [[PubMed](#)]
18. Bakare, F.F.; Chou, Y.-J.; Huang, Y.-H.; Tesfay, A.H.; Moriga, T.; Shih, S.-J. Correlation of morphology and in-vitro degradation behavior of spray pyrolyzed bioactive glasses. *Materials* **2019**, *12*, 3703. [[CrossRef](#)] [[PubMed](#)]
19. Chou, Y.-J.; Ningsih, H.S.; Shih, S.-J. Preparation, characterization and investigation of antibacterial silver-zinc co-doped β -tricalcium phosphate by spray pyrolysis. *Ceram. Int.* **2020**, *46*, 16708–16715. [[CrossRef](#)]
20. Janackovic, D.; Jokanovic, V.; Kostic-Gvozdenovic, L.; Zec, S.; Uskokovic, D. Synthesis and formation mechanism of submicrometre spherical cordierite powders by ultrasonic spray pyrolysis. *J. Mater. Sci.* **1997**, *32*, 163–168. [[CrossRef](#)]
21. Messing, G.L.; Zhang, S.C.; Jayanthi, G.V. Ceramic powder synthesis by spray pyrolysis. *J. Am. Ceram. Soc.* **1993**, *76*, 2707–2726. [[CrossRef](#)]
22. Chen, J.; Yang, H.; Xu, C.-M.; Cheng, J.-G.; Lu, Y.-W. Preparation of ZrO₂ microspheres by spray granulation. *Powder Technol.* **2021**, *385*, 234–241. [[CrossRef](#)]
23. Chen, L.G.; Huang, Y.H.; Chou, Y.J. Preparation and characterization of spray-dried granulated bioactive glass micron spheres. *Int. J. Appl. Ceram. Technol.* **2021**, *18*, 1743–1750. [[CrossRef](#)]
24. Sosnik, A.; Seremeta, K.P. Advantages and challenges of the spray-drying technology for the production of pure drug particles and drug-loaded polymeric carriers. *Adv. Colloid Interface Sci.* **2015**, *223*, 40–54. [[CrossRef](#)]
25. Nandiyanto, A.B.D.; Ogi, T.; Wang, W.-N.; Gradon, L.; Okuyama, K. Template-assisted spray-drying method for the fabrication of porous particles with tunable structures. *Adv. Powder Technol.* **2019**, *30*, 2908–2924. [[CrossRef](#)]

26. Grigoriev, S.N.; Soe, T.N.; Malakhinsky, A.; Makhadilov, I.; Romanov, V.; Kuznetsova, E.; Smirnov, A.; Podrabinnik, P.; Khmyrov, R.; Solís Pinargote, N.W. Granulation of Silicon Nitride Powders by Spray Drying: A Review. *Materials* **2022**, *15*, 4999. [CrossRef]
27. Nampi, P.P.; Kume, S.; Hotta, Y.; Watari, K.; Itoh, M.; Toda, H.; Matsutani, A. The effect of polyvinyl alcohol as a binder and stearic acid as an internal lubricant in the formation, and subsequent sintering of spray-dried alumina. *Ceram. Int.* **2011**, *37*, 3445–3450. [CrossRef]
28. Tosaka, M.; Murakami, S.; Poompradub, S.; Kohjiya, S.; Ikeda, Y.; Toki, S.; Sics, I.; Hsiao, B.S. Orientation and crystallization of natural rubber network as revealed by WAXD using synchrotron radiation. *Macromolecules* **2004**, *37*, 3299–3309. [CrossRef]
29. King, P.; McMillan, P.; Moore, G.; Ramsey, M.; Swayze, G. Infrared spectroscopy of silicate glasses with application to natural systems. *Infrared Spectrosc. Geochem. Explor. Geochem. Remote Sens.* **2004**, *33*, 93–133.
30. Siddharthan, A.; Seshadri, S.; Kumar, T.S. Microwave accelerated synthesis of nanosized calcium deficient hydroxyapatite. *J. Mater. Sci. Mater. Med.* **2004**, *15*, 1279–1284. [CrossRef]
31. Nahar, U.; Shovon, B.; Chandra, R.; Shukanta, B.; Chandra, S. Characterization of beta-tricalcium phosphate (β -TCP) produced at different process conditions. *J. Bioeng. Biomed. Sci.* **2017**, *7*, 2. [CrossRef]
32. Wallin, R.F.; Arscott, E. A practical guide to ISO 10993-5: Cytotoxicity. *Med. Device Diagn. Ind.* **1998**, *20*, 96–98. Available online: https://www.namsa.com/wp-content/uploads/2015/10/A-Practical-Guide-to-ISO-10993-5_Cytotoxicity.pdf (accessed on 26 February 2021).
33. Bellucci, D.; Cannillo, V.; Sola, A. Coefficient of thermal expansion of bioactive glasses: Available literature data and analytical equation estimates. *Ceram. Int.* **2011**, *37*, 2963–2972. [CrossRef]
34. Tsuru, Y.; Shinzato, Y.; Saito, Y.; Shimazu, M.; Shiono, M.; Morinaga, M. Estimation of linear thermal expansion coefficient from cohesive energy obtained by ab-initio calculation of metals and ceramics. *J. Ceram. Soc. Jpn.* **2010**, *118*, 241–245. [CrossRef]
35. Sivamma, M.; Snehitha, R. Atomization techniques in spray drying: A Review. *Pharma Innov. J.* **2021**, *10*, 454–461.
36. Ningsih, H.S.; Tannesia, L.; Chen, H.-H.; Shih, S.-J. Fabrication, characterization and in vitro cytotoxicity of mesoporous β -tricalcium phosphate using the spray drying method. *Crystals* **2021**, *11*, 252. [CrossRef]
37. Naz, S.; Gul, A.; Zia, M. Toxicity of copper oxide nanoparticles: A review study. *IET Nanobiotechnol.* **2020**, *14*, 1–13. [CrossRef]
38. Addison, W.N.; Azari, F.; Sørensen, E.S.; Kaartinen, M.T.; McKee, M.D. Pyrophosphate inhibits mineralization of osteoblast cultures by binding to mineral, up-regulating osteopontin, and inhibiting alkaline phosphatase activity. *J. Biol. Chem.* **2007**, *282*, 15872–15883. [CrossRef]

Disclaimer/Publisher’s Note: The statements, opinions and data contained in all publications are solely those of the individual author(s) and contributor(s) and not of MDPI and/or the editor(s). MDPI and/or the editor(s) disclaim responsibility for any injury to people or property resulting from any ideas, methods, instructions or products referred to in the content.